Crystallization behavior of non-stoichiometric Ge–Bi–Te ternary phase change materials for PRAM application

2007 J. Phys.: Condens. Matter 19 446004

(http://iopscience.iop.org/0953-8984/19/44/446004)

IOP PUBLISHING JOURNAL OF PHYSICS: CONDENSED MATTER

J. Phys.: Condens. Matter **19** (2007) 446004 (9pp) doi:10.1088/0953-8984/19/44/446004

Crystallization behavior of non-stoichiometric Ge–Bi–Te ternary phase change materials for PRAM application

C W Sun[1], M S Youm[2] and Y T Kim[2]

[1] Department of Materials Science and Engineering, Korea Advanced Institute of Science and Technology, Daejeon 305-701, Korea
[2] Semiconductor Materials and Devices Laboratory, Korea Institute of Science and Technology, Seoul 136-791, Korea

E-mail: suxxus@kaist.ac.kr

Received 21 June 2007, in final form 9 August 2007
Published 24 September 2007
Online at stacks.iop.org/JPhysCM/19/446004

Abstract

We investigated the properties of a Ge–Bi–Te ternary chalcogenide thin film which was deposited on a SiO_2/Si substrate by varying RF-sputtering power on the GeTe and Bi target. The aim was to search for an appropriate candidate for a new phase change memory. Various analyses are conducted in order to investigate the composition, phase separation, and crystallization behavior of the Ge–Bi–Te alloy. The XRD results of each annealed sample showed that the Ge–Bi–Te alloy crystallized into $Ge_2Bi_2Te_5$, $GeBi_2Te_4$, $GeBi_4Te_7$ phase at around 300 °C according to Ge content and expelled amorphous Ge crystallized as a single phase over 400 °C. Combining these with the differential scanning calorimetry (DSC) results, we demonstrated that T_c and T_m of the Ge–Bi–Te alloy are respectively higher and lower than those of conventional Ge–Sb–Te (GST) films. All the phases, including not only various Ge–Bi–Te ternary phases but also the Ge phase crystal structure, were also confirmed with high-resolution transmission electron microscopy (HR-TEM) images and diffraction patterns. It is noted that some of the $Ge_2Bi_2Te_5$ grains show specific facetted planes such as {0113}, {0112}, and {0001}. Through successive analyses, we revealed the structural evolution of the Ge–Bi–Te alloy according to Ge contents and confirmed the potential of the Ge–Bi–Te alloy for phase-change random access memory (PRAM) applications.

(Some figures in this article are in colour only in the electronic version)

1. Introduction

Recently, among many other chalcogenide amorphous semiconductors, the Ge–Sb–Te (GST) system has been studied intensively for phase change memory, because of fast crystallization

and better data storage lifetime characteristics [1]. However, for achievement of high density commercial memory devices, some problems have to be solved, such as the high current pulse required for the amorphization process, because the sample must be heated to its melting point during the reset operation. Therefore, the critical issues in phase change material requirements are summarized as follows: stability at room temperature, high crystallization speed, and reduction of writing currents. Until now, many groups have tried to work out the above problems in various ways. Research into changing crystallization behavior by typical elements doping into GST, especially the $Ge_2Sb_2Te_5$ alloy [2], and decreasing the power consumption by reducing the area of the bottom-electrode contact (BEC) is being carried out. However, in the former method, there have not been any promising developments, and in the latter research, the required area has been much smaller than for the respective process node [3, 4]. Therefore, fundamental research for an alternative GST phase change material is crucial. In this paper, as a new alternative for the well known GST, a Ge–Bi–Te (GBT) alloy is now suggested because the Bi, which lies in same group as Sb but has larger atomic radius ($r_{Bi} = 0.163$ nm, $r_{Sb} = 0.153$ nm), has been regarded as increasing the crystallization speed [5]. Recently, Matsunaga *et al* [6] reported that replacement of a proportion of Sb atoms in the pseudo-binary system—GeTe–Sb_2Te_3—with Bi results in faster crystallization. They explained the reason as follows; the GBT alloy in a pseudo-binary line is crystallized into a metastable simple cubic structure with $P\bar{3}m1$ space group. The structure with randomly distributed Ge, Bi, Te atoms in the 1(a) site more closely resembles an amorphous structure than the NaCl structure of GST and this assures the more rapid phase transition from the amorphous to crystalline phase and vice versa. Moreover, the Ge has been known to increase the crystallization temperature due to its strong inter-atomic bonding strength. Therefore, with the aim of checking the possibility as an alternative phase change memory material, a ternary GBT system co-sputtered by different RF power is investigated.

2. Experimental details

RF-sputtered amorphous Ge–Bi–Te (GBT) ternary chalcogenide film with a thickness of 200 nm was deposited on a SiO_2/Si(100) substrate for the purpose of avoiding the substrate effects of an Si single crystal on the crystallization of GBT thin films. The deposition rate was 30 nm min^{-1} by sputtering a $Ge_{64}Te_{36}$ and Bi single target with different power in Ar ambient where the working pressure and base pressures were 1.5 and 1.2×10^{-3} mTorr, respectively. The reason why we used the Ge-rich $Ge_{64}Te_{36}$ target is such that the strong cohesive Ge inter-atomic force seems to increase the crystallization temperature of the GBT alloy. The composition was controlled by controlling the RF sputtering powers on each target which are 70 W:20 W, 70 W:30 W, and 70 W:40 W (hereafter, we called each sample GBT20, GBT30, GBT40). The constituent profile of each sample was confirmed with auger electron spectroscopy (AES) after deposition. The decrement of Ge contents with increasing Bi target sputtering power is expected. The crystallization and melting temperatures were measured by using differential scanning calorimetry (DSC). Based on the measured T_{crys}, we carried out a rapid thermal annealing (RTA) process under N_2 ambient conditions at 150, 300, and 400 °C for 1 min in order to observe the crystallization behavior and progressive change of grain shape with temperature. We conducted the x-ray diffraction (XRD) analysis for each annealed sample with fixed θ ($\theta = 3°$, 2θ scan) at 30 kV, 60 mA condition using a Rigaku, D/mas-rc (12 kW). Generally, a 2θ scan is used for increasing the amount of x-ray on the thin film. We used this method in order to obtain as many diffracted peaks as possible for confirming the phase. Cross-sectional TEM specimens were prepared by the conventional method followed by ion-milling with Ar ions. Ion milling was performed using the liquid nitrogen cooling stage of a Fischione

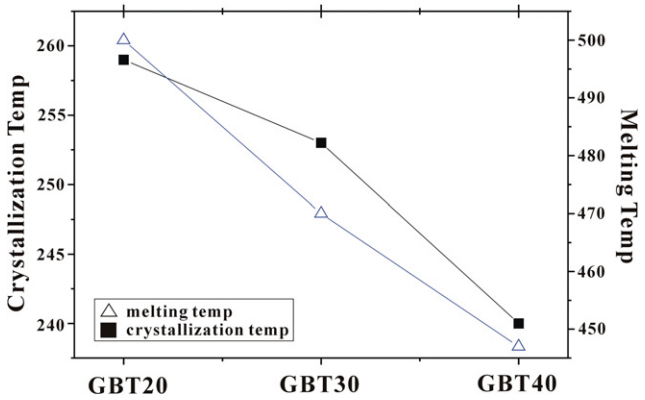

Figure 1. Crystallization and melting temperatures of GBT20, GBT30, and GBT40 samples measured by DSC.

1010 ion miller with conditions of 4 kV and 4 mA to suppress the unwanted crystallization by sample heating during the conventional Ar ion milling without cooling. Selected area electron diffraction (SAED) patterns and high-resolution transmission electron microscopy (HR-TEM) images were obtained with a JEOL JEM-2000EX operated at 200 kV and a JEM-3010 operated at 300 kV.

3. Results and discussion

According to the GBT ternary alloy phase diagram, GBT alloy is crystallized into a similar composition as the Ge–Sb–Te ternary alloy, i.e. 1:2:4, 2:2:5, 1:4:7, etc. These compositions lie along the pseudo-binary line of $GeTe–Bi_2Te_3$. Therefore we assume that the RF-power modulated GBT alloy crystallized into one of the stable phases in the pseudo-binary line. Firstly, we tried to confirm the constitution of each alloy. According to the AES results of as-deposited alloys, relative Ge contents of each sputtered alloy decreased from 53 at.% to 46 at.% to 43 at.% as the sputtering power on the Bi target increased. We expected the structural changes from Ge-rich type to Ge-less type alloy with deposition condition variation. However, these compositions did not seem to be satisfied with the known stoichiometric GBT alloy. In general, there exist two possible transformation mechanisms according to the composition of the amorphous state [7]. In the case of stoichiometric composition, the crystallization growth mechanism is thought to be a eutectic-interface extension, which is so-called diffusionless crystallization—growth dominant crystallization. Contrarily, in the case of non-stoichiometric composition like the above GBT alloy, due to the density gradients of atoms, the crystallization is accompanied by long range atomic diffusion as well as phase separation and follows a nucleation and growth transformation mechanism—nucleation dominant crystallization. Therefore, the activation energy shows a large value and diffusion requires a long annealing time for crystallization at high temperature close to the melting temperature. The sputtered GBT alloy seems to follow the latter transformation mechanism.

We also conducted differential scanning calorimetry (DSC) measurements. In figure 1, the crystallization and the melting temperatures of sputtered GBT alloys (GBT20, GBT30, GBT40) are shown as 259 °C, 254 °C, 240 °C and 500 °C, 470 °C, 450 °C, respectively. The T_c and T_m of pure Ge are known as 500 °C, 937 °C and those of GBT ternary alloys—$GeBi_2Te_4$, $GeBi_4Te_7$—are identified as below 200 °C, near 600 °C–587 °C, 576 °C [8, 9]. Ge interatomic bonding strength (263.6 kJ mol^{-1}) is higher than those of Bi (200.4 kJ mol^{-1}) and

Te (259.8 kJ mol^{-1}). In addition, Ge is well-known as one of the most effective material in increasing the T_g (the glass transition temperature), because its high coordination number (4) increases the average coordination number and bond enthalpy in the phase change material [10]. In earlier reports of excess Ge doped GST material [11], Privitera *et al* recount that after the formation of a maximum fraction crystallite of the GST phase, the crystallization rate is strongly reduced, and a further conversion of the film into a crystalline structure can occur only by increasing the annealing temperature. Therefore, Ge seems to suppress the crystallization of stoichiometric GBT alloy and this would be the reason for the high crystallization temperature. These DSC results roughly support the possibility of GBT alloy for PRAM application because the crystallization and the melting temperatures are higher and lower than those of the GST-225(151–174 °C, 632 °C) alloy which is known as the most promising material for PRAM. It is thought that high crystallization temperature guarantees the stability at room temperature, and low melting temperature ensures a reduction in the writing current during the reset operation of PRAM. Generally, contradiction between speed and stability of phase change material is commonly solved by sacrificing speed so as to ascertain the stability. Compared with conventional GST properties, we expected both the improvement of crystallization speed by Bi and advancement of stability by Ge. However, Ge has more effect on the properties of GBT alloy than Bi. With regard to the crystallization speed of sputtered GBT alloy, those of GBT20, GBT30, and GBT40 alloys are slower than that of GST. Because, $\Delta T = T_m - T_x$ values of all GBT alloys which are proportional to the driving force for crystallization depicted as $-\Delta Gv = \Delta H_f \Delta T / T_m$ are smaller than that of GST. Consequently, the sputtered GBT alloy attained more stability than preexisting GST with increased crystallization temperature and lowered melting temperature. It is thought that we have made a good compromise between the two counter factors.

In figure 2, we show XRD results of each sample. Figure 2(a) represents the series XRD features of GBT20 samples which are for the as-deposited one as well as the annealed one at 150 °C and 300 °C for 1 min. The GBT20 alloy maintains the amorphous state until 150 °C. At 300 °C, the observed crystalline peaks were confirmed as $Ge_2Bi_2Te_5$ phase. Commonly, GBT ternary alloy structure can be inferred from the GeTe–Bi_2Te_3 pseudo-binary system and all the intermediate stable structures are explained by the nGeTe–mBi_2Te_3 form [12]. Therefore, intermediate structures can be divided into two parts, the GeTe-rich region and the Bi_2Te_3-rich region. Compositions of 5:2:8, 4:2:7, 3:2:6, 2:2:5, 1:2:4 can be shown in the former region and 1:4:7, 1:6:10, 1:8:13 in the latter region. Among them, the well-known stable composition structures are $Ge_2Bi_2Te_5$ ($n = 2, m = 1$), $GeBi_2Te_4$ ($n = 1, m = 1$), $GeBi_4Te_7$ ($n = 1, m = 2$) [13]. The $Ge_2Bi_2Te_5$ unit cell ($a = 0.4286$ nm, $c = 1.7394$ nm, space group is $P\bar{3}m1$) consists of one nine-layer packet—TeMeTeMeTeTeMeTeMe—(Me is mixed Bi/Ge layer) with $N = 9$, where N is the number of atomic layers along the c-axis per unit cell. Similarly, the $GeBi_2Te_4$ unit cell ($a = 0.4322$ nm, $c = 4.172$ nm, space group is $R\bar{3}m$) consists of three seven-layer packets—TeMeTeMeTeTeMe—(Me is mixed Bi/Ge layer) with $N = 21$. In these two phases, the structures are very similar, e.g. the (0009) inter-planar spacing of $Ge_2Bi_2Te_5$, 0.1983 nm, is akin to the $GeBi_2Te_4$(00021) spacing, 0.1965 nm. Thus, the Bragg diffraction will occur a at similar angle. In figure 2(c), simulated XRD patterns of $GeBi_4Te_7$, $GeBi_2Te_4$, and $Ge_2Bi_2Te_5$ structures, four of the most intensive diffracted peak positions of $GeBi_2Te_4$ and $Ge_2Bi_2Te_5$ are very alike (#1—28.22°, 28.55°, #2—38.85°, 39.47°, #3—41.76°, 41.71°, #4—51.17°, 51.68°). Moreover, similar polytypical phases formed by the weak van der Waals forces usually show very small energy differences that can cause various crystallographic transitions [14]. Therefore, $GeBi_2Te_4$ and $Ge_2Bi_2Te_5$ phases are seen to co-exist at 300 °C for the annealed GBT20 alloy. According to Karpinsky *et al* [15], significant changes in the number of N layers per unit cell are observed with increasing excess of Ge

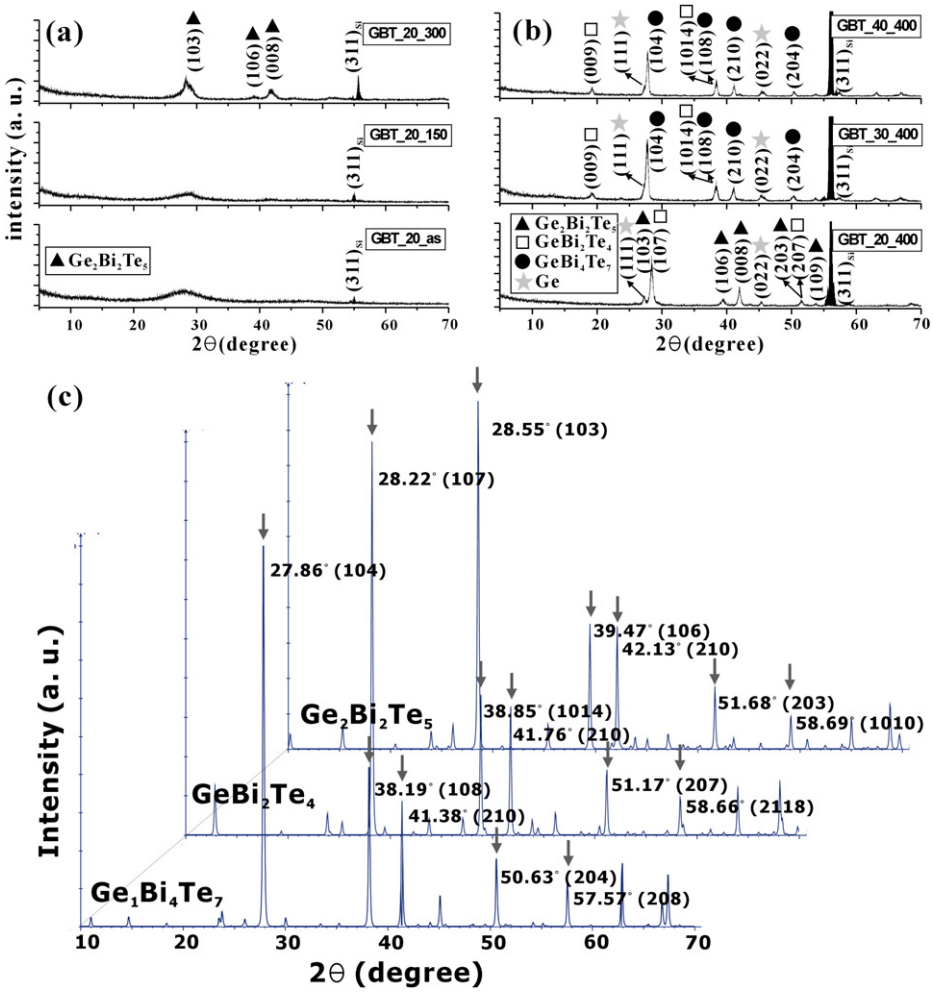

Figure 2. X-ray diffraction data of (a) GBT20 samples at as-deposited state, 150 °C, 300 °C and (b) 400 °C annealed GBT20, GBT30, and GBT40. (c) Simulated XRD patterns of $Ge_2Bi_2Te_5$, $GeBi_2Te_4$, and $GeBi_4Te_7$ alloy.

for the alloys of $GeBi_2Te_4 + Ge$ and $GeBi_4Te_7 + Ge$. The former changes to $Ge_2Bi_2Te_5$ and the latter transforms to $GeBi_2Te_4$ and $Ge_2Bi_2Te_5$. Conversely, this means that GBT20, which shows the largest Ge content among sputtered samples, firstly crystallize into the $Ge_2Bi_2Te_5$ (23 at.% Ge) phase. As temperature increases, excess Ge come out and crystallizes as a single phase and the remaining $Ge_2Bi_2Te_5$ transforms into $GeBi_2Te_4$ (14 at.% Ge). GBT30, GBT40 with relatively less Ge content crystallize into the $GeBi_4Te_7$ (8.3 at.% Ge) phase. XRD data of 400 °C annealed GBT30 and GBT40 in figure 2(b) show that $GeBi_2Te_4$ and $GeBi_4Te_7$ exist together. It is known that the phase separation during crystallization must be accompanied by slow diffusion of atomic species, which limits the crystallization speed and is the main cause of deterioration of memory devices [16–19]. However, Liu *et al* [20] reported that phase separation increased the resistance due to current carrier scattering by the crystalline boundary. In this experiment, we did not find significant worsening in properties of the films caused by phase separation.

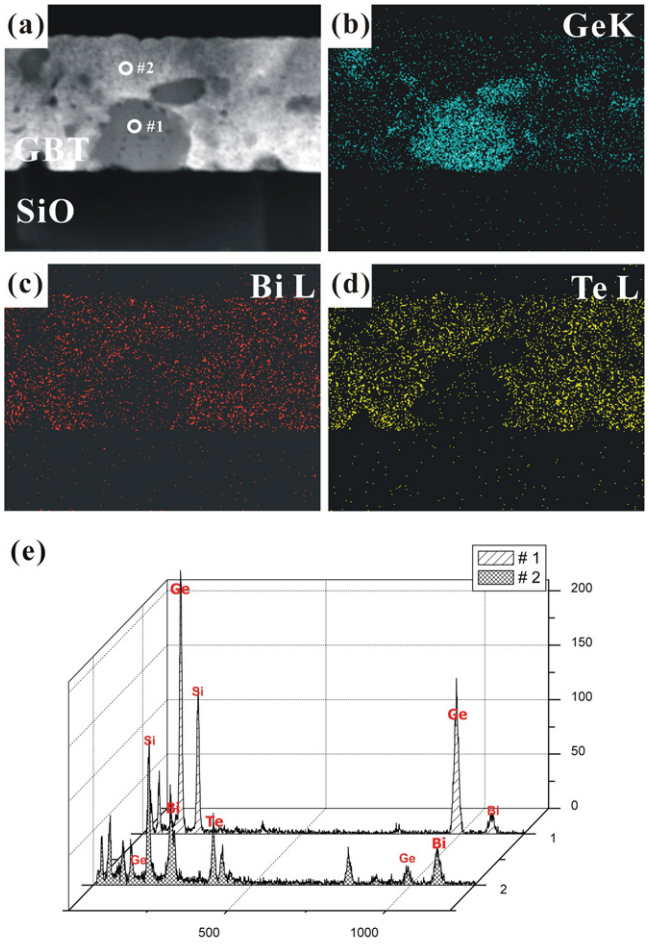

Figure 3. (a) High angle annular dark-field image of 400 °C annealed GBT20 sample and (b)–(d) corresponding energy dispersive spectroscopy (EDS) elemental mapping images. (e) EDS data of the neighboring region in thin films marked #1 and #2 in figure 3(a).

The existence of the Ge phase was confirmed with energy dispersive spectroscopy (EDS) experiments with the 400 °C annealed GBT20 sample. Mapping results of each element (Ge, Bi, Te) are presented in figure 3. The nearest two grains show a different composition ratio, one of which is Ge dominant (#1) and the other is Bi–Te dominant (#2). This result supports the result that excess of Ge atoms diffuse out from the GeTe-rich type GBT grains like $GeBi_2Te_4$ or $Ge_2Bi_2Te_5$ and crystallize over 400 °C. Thus this phenomenon affects the crystallization and melting temperature of sputtered GBT alloy. We think that more detailed research of the Ge phase effect on the GBT alloy properties will be needed. In figure 4, bright-field transmission electron microscopy (BF-TEM) images and corresponding diffraction patterns of annealed GBT20 sample are shown. Overall results such as amorphous phase preservation up to 150 °C, the co-existence of GBT ternary crystallite and residual amorphous Ge phase over 300 °C (diffraction spots with halo rings), and the appearance of the crystalline Ge phase at 400 °C all coincide with XRD data. In figures 4(c) and (d), the size of crystalline grains in

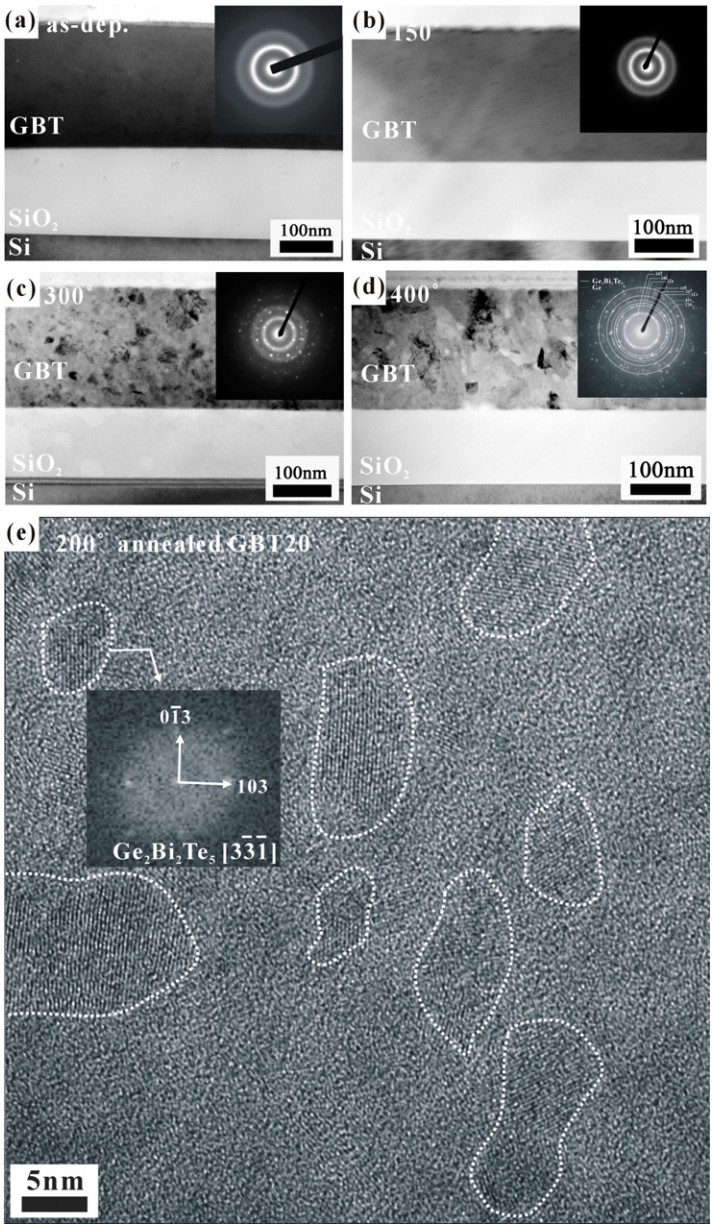

Figure 4. BF-TEM images and corresponding diffraction patterns of the GBT20 sample. (a) As-deposited state, annealed at (b) 150 °C (c) 300 °C, and (d) 400 °C for 1 min are shown. (e) HR-TEM image of the 200 °C annealed GBT20 sample which represents competitive small nuclei formation.

300 °C and 400 °C annealed samples varies from several nm to 100 nm. Furthermore, the high resolution image of 200 °C annealed GBT20 in figure 4(e) represents crystallization initiated by randomly formed small nuclei. From these results, we deduced that the crystallization follows the nucleation-growth mechanism—crystallization proceeds mainly via the generation of small nuclei which are sufficiently large and grow competitively over 400 °C.

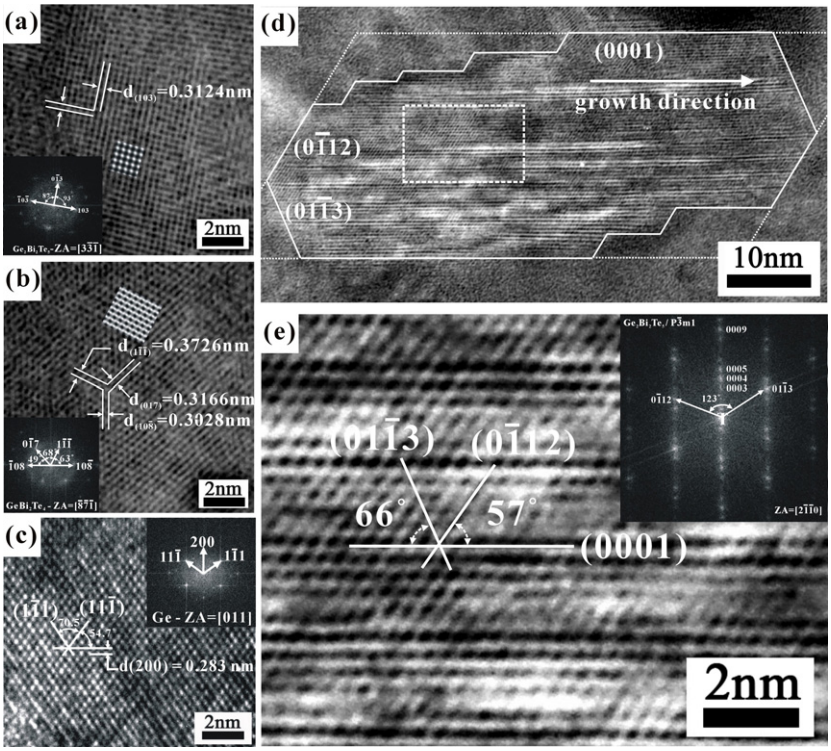

Figure 5. HR-TEM images of $Ge_2Bi_2Te_5$, $GeBi_2Te_4$, Ge phase observed at 400 °C for the annealed sample viewed along (a) $Ge_2Bi_2Te_5$-[3$\bar{3}\bar{1}$], (b) $GeBi_2Te_4$-[$\bar{8}\bar{7}\bar{1}$], (c) Ge-[011] directions are shown with simulated image. (d) HR-TEM image of ⟨2110⟩ zone-axis $Ge_2Bi_2Te_5$ phase is shown in which we verify the atomic layer structure and inter-planar angles. (e) Enlarged image of rectangular area in figure 5(d).

In figure 5, we show the HR-TEM images of 400 °C annealed samples in order to unravel the accurate structure and phase. We superimposed the image simulated with NCEM (National Center for Electron Microscopy) software with adequate defocus and thickness conditions on each image. As mentioned above, the GBT ternary alloy structures generally show the layered structure in the rhombohedral Bravais lattice. Therefore, in order to investigate the atomic layer sequence of a rhombohedral structured alloy, one should view the structure along the ⟨2110⟩ or ⟨0110⟩ direction. However, including the *a*-axis direction, ⟨2110⟩, GBT ternary structures are observed along the high index zone axis—[3$\bar{3}\bar{1}$], [$\bar{8}\bar{7}\bar{1}$]. Actually, the atomic arrangement along viewing directions in figures 5(a) and (b) is very symmetrical to get a high resolution image. In figure 5(c), the Ge phase observed in 400 °C annealed alloy is shown. Figure 5(d) depicts several tens of nm-sized specific grains annealed at 300 °C, which are viewed along the ⟨2110⟩ direction. The growth direction of the grain is ⟨0001⟩. Note that specific facetted planes like {0112}, {0113}, and {0001} are observed. The appearance of characteristic facetted planes have been reported before in GST-225 alloy [21]. According to the broken bond model [22], only two planes having the lowest surface energy—{0001}, {0112}—can remain, and the highest surface energy plane among them—{0113}—will vanish as the crystallization goes on. The expected grain shape is represented by a dotted line.

4. Conclusion

We conducted the compositional analysis and structural characterization of series annealed Ge–Bi–Te ternary phase change material. Through AES analysis, we confirmed that the elemental composition of as-deposited film showed a non-stoichiometric constitution. XRD results of the 400 °C annealed sample showed the existence of various Ge–Bi–Te ternary phases along the Bi_2Te_3–GeTe pseudo-binary line. As the relative amount of Ge decreases from GBT20 (53 at.% Ge) to GBT30 (46 at.% Ge) to GBT40 (43 at.% Ge), ternary alloy composition varies from $Ge_2Bi_2Te_5$ to $GeBi_2Te_4$ to $GeBi_4Te_7$ with excess of Ge phase. Moreover, EDS results manifested the reason for the appearance of the Bi–Te-rich phase with increasing annealing temperature; the formation of the GeTe-rich ternary alloy was less favored than the separation of the Ge phase and the Bi–Te-rich phase. Through TEM analysis, we showed the initiation of crystallite formation and that the crystallization of GBT alloy occurred mainly by a nucleation-growth mechanism. In addition, every phase existing in the GBT alloy was confirmed by HR-TEM images viewed along various zone axes. Furthermore, from the specific facet planes, we predicted the grain growth direction—[0001]—and the final stable structure with energetically favorable planes—{0001}, {0112} planes.

Acknowledgments

This work was supported by Samsung Electronics and the Korean Ministry of Commerce, Industry, and Energy (MOCIE) under the National Research Project of Phase-Change Random Access Memory Development.

References

[1] Gill M, Lowrey T and Park J 2002 *IEEE ISSCC Dig. Tech. Pap.* p 202
[2] Matsuzaki N, Kurotsuchi K, Matsui Y, Tonomura O, Yamamoto N, Fujisaki Y, Kitai N, Takemura R, Osada K, Hanazawa S, Moriya H, Iwasaki T, Kawahara T, Takaura N, Terao M, Matsuoka M and Moniwa M 2005 *IEDM Technical Digest* p 738
[3] Ahn S J, Hwang Y N, Song Y J, Lee S H, Lee S Y and Park J H 2005 *Symp VLSI Tech, Tech Dig* pp 98–9
[4] Cho S L, Yi J H, Ha Y H, Kuh B J, Lee C M and Park J H 2005 *Symp. VLSI Tech, Tech. Dig.* pp 96–7
[5] Wang K, Wamwangi D, Ziegler S, Sfteimer C and Wuttig M 2004 *J. Appl. Phys.* **96** 5557–62
[6] Matsunaga T and Yamada N 2004 *Japan. J. Appl. Phys.* **43** 4704–12
[7] Situ H, Wang Z T and Jung A L 1989 *J. Non-Cryst. Solids* **113** 88–93
[8] Chambouleyron I, Fajardo F and Janatta A R 2002 *J. Non-Cryst. Solids* **299** 143–7
[9] Skoropanov A S, Walewski B L, Samal G L, Alfer S A and Wetscher A A 1987 *Z. Phys. Chem.* **268** 97
[10] Lankhorst M H R 2002 *J. Non-Cryst. Solids* **297** 210–9
[11] Privitera S, Rimini E, Bongiorno C, Zonca R, Pirovano A and Bez R 2003 *J. Appl. Phys.* **94** 4409–13
[12] Shelimova L E, Carpinskii O G, Konstantinov P P, Avilov E S, Kretova M A and Zemskov V S 2004 *Inorg. Mater.* **405** 451–60
[13] Shelimova L E, Konstantinov P P, Karpinsky O G, Avilov E S, Kretova M A and Zemskov V S 2001 *J. Alloys Compounds* **329** 50–62
[14] Kuznetsova L A, Kuznetsov V L and Rowe D M 2000 *J. Phys. Chem. Solids* **61** 1269–74
[15] Karpinsky O G, Shelimova L E, Kretova M A and Fleurial J-P 1997 *J. Alloys Compounds* **265** 170–5
[16] Nakayama K, Kojima K, Hayakawa F, Imai Y, Kitagawa A and Suzuki M 2000 *Japan. J. Appl. Phys.* **39** 6157–61
[17] Privitera S, Rimini E, Bongiorno C, Zonca R, Pirovano A and Bez R 2003 *J. Appl. Phys.* **94** 4409–13
[18] Coombs J H, Jongenelis A P J M, van Es-Spiekman W and Jacobs B A 1995 *J. Appl. Phys.* **78** 4918–28
[19] Chem M, Rubin K A and Barton R W 1986 *Appl. Phys. Lett.* **49** 502–4
[20] Liu B, Song Z, Feng S and Chen B 2005 *Mater. Sci. Eng.* B **119** 125–30
[21] Park Y J, Lee J Y and Kim Y T 2006 *Appl. Phys. Lett.* **88** 201905–7
[22] Porter D A and Easterling K E 1992 *Phase Transformations in Metals and Alloys* (London: Chapman and Hall)